J. Plasma Physics (1997), *vol.* 57, *part* 1, *pp.* 35–45

Copyright © 1997 Cambridge University Press

Transition to turbulent electric current sheet reconnection

RUSSELL B. DAHLBURG

Laboratory for Computational Physics and Fluid Dynamics, Naval Research Laboratory, Washington, DC 20375-5344, USA

(Received 11 March 1996)

Electric current sheets develop in the solar corona when different flux systems come into contact. At these sheets magnetic energy is transformed into heat and kinetic energy by means of reconnection. We have previously demonstrated how to accelerate neutral sheet energy conversion by means of a transition to turbulent reconnection via ideal, three-dimensional secondary instabilities, as conjectured by Montgomery. In this paper we describe how our previous results are modified by the presence of a finite mean sheetwise magnetic field. We find a stabilization from this field, due to a decrease in energy transfer from the basic magnetic field to the three-dimensional perturbed fields. An increase in perturbed dissipative energy losses is also observed.

1. Introduction

The conversion of magnetic energy into heat and kinetic energy in the solar corona is a problem of longstanding interest. A problem has been that classical analyses indicate that the rate at which magnetic energy is converted is too slow to account for many of the phenomena that are observed in the corona, e.g. in coronal heating. Another problem has been to substantiate the hypothesis that magnetic reconnection might be responsible for processes with widely varying time scales, such as the onset, impulsive and decay phases of a two-ribbon solar flare. The problem here is related to the first one, in that the very energetic impulsive phase is the difficult one to explain.

Hence it has been of interest to determine ways in which this magnetic energy conversion rate can be increased. One hypothesis is that reconnection can become turbulent, and that turbulent reconnection will proceed at a rate faster than 'laminar' magnetic reconnection (Strauss 1986, 1988). It was suggested by Montgomery (1984, 1989) that to understand the transition to turbulent magnetic reconnection a profitable approach would be to adapt a technique used with great success for hydrodynamic problems, namely the transition to turbulence via secondary instabilities. This is a three-step process in which

(A) a one-dimensional primary basic state is destabilized by a two-dimensional primary linear disturbance;
(B) the primary linear disturbance saturates and a two-dimensional secondary equilibrium state develops;
(C) the two-dimensional secondary equilibrium state is itself destabilized by a three-dimensional, ideal secondary instability.

When this secondary mode attains a large amplitude, the particular system can

https://doi.org/10.1017/S0022377896005247 Published online by Cambridge University Press

then become turbulent, turbulence being understood as an enhanced generation of small-scale structure and chaotic behaviour of the local flow variables. This approach has been useful in studying a variety of flows, including plane Poseuille and plane Couette flows, flat-plate boundary layers (Orszag and Patera 1983) and free-shear layers (Metcalfe *et al*. 1987). Hence we attacked the magnetic reconnection problem by first formulating a magnetohydrodynamic generalization of the Orr–Sommerfeld equation to the neutral sheet (Dahlburg *et al*. 1983), which we then solved with a Chebyshev-tau method (Orszag 1971) to determine the character of the primary disturbances. We subsequently examined the nonlinear saturation of the neutral sheet in two spatial dimensions (Dahlburg *et al*. 1986). A preliminary attack on the transition-to-turbulence problem was made in a triply periodic geometry (Montgomery *et al*. 1987) in which a laminar breakdown was observed. A full attack on the problem was made later (Dahlburg *et al*. 1992). In that paper it was shown that this hypothesis is correct for neutral sheets, in which reconnection can proceed to turbulence via ideal, three-dimensional secondary instabilities. We applied the theory to the case of two-ribbon solar flares, and showed that the various phases of the solar flare could be examined by different stages in the transition to turbulence (Dahlburg *et al*. 1993). The theory was subsequently generalized to include flows (Dahlburg and Karpen 1994*a*, *b*) and used for an examination of transition to turbulence in solar surges (Carbone *et al*. 1987).

In this paper we examine, as an example of the secondary instability theory, the transition to turbulent magnetic reconnection of a three-dimensional (3D) electric current sheet. Our concern here is with how the addition of a sheetwise magnetic field component will affect our earlier results. This new configuration, generally termed an electric current sheet, occurs when regions of obliquely directed magnetic field are brought together. This happens, for example, when magnetic flux emerges into the upper solar atmosphere and comes into contact with the pre-existing magnetic field. However, a sheetwise magnetic field can often provide a strong stabilizing effect, for example for kink instabilities. A strong enough sheetwise magnetic field might stabilize the secondary mode completely.

In this paper we shall show that, for many sheetwise field strengths, the electric current sheet does have a secondary mode. However, the mode can be stabilized for large enough magnitudes of this field. An examination of the energetics shows that the stabilization occurs owing to a hindrance of energy transfer between the one-dimensional (1D) and 3D fields.

In Sec. 2 we lay out the equations, boundary conditions and initial conditions that we shall study. Our numerical simulations are discussed in Sec. 3. Section 4 details our conclusions.

2. Setting up the problem

We want to investigate the evolution of a three-dimensional electric current sheet perturbed by two- and three-dimensional disturbances. Hence we initialize the magnetic field in the following way:

$$\mathbf{B}(x,y,z,t=0) = B_{0x}(z)\,\hat{\mathbf{e}}_x + B_{0y}(z)\,\hat{\mathbf{e}}_y + \epsilon_{2D}\,\mathbf{B}_{2D}(z)\,e^{i\alpha x} + \epsilon_{3D}\,\mathbf{B}_{3D}(z)\,e^{i\alpha(x+\phi)+i\beta y}, \tag{1a}$$

https://doi.org/10.1017/S0022377896005247 Published online by Cambridge University Press

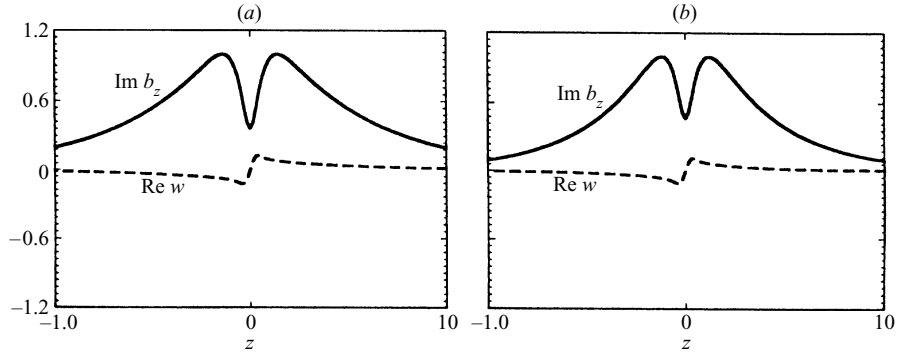


Figure 1. Primary unstable eigenfunctions as functions of the cross-sheet coordinate z for $\alpha = 0.2$, $S = S_v = 10^3$: (*a*) two-dimensional mode ($\beta = 0$) for $\omega = (0, 0.0138)$; (*b*) three-dimensional mode ($\beta = 0.2$) for $\omega = (0, 0.0105)$. Here Re w is the real part of the cross-sheet velocity, and Im b_z is the imaginary part of the cross-sheet perturbed magnetic field.

where $B_{0x}(z)\,\hat{\mathbf{e}}_x$ is the mean field in the x direction, $B_{0y}(z)\,\hat{\mathbf{e}}_y$ is the mean field in the y direction, ϵ_{2D} is the amplitude of the two-dimensional unstable primary eigenmode ($\mathbf{B}_{2D}$), ϵ_{3D} is the amplitude of the three-dimensional unstable primary eigenmode ($\mathbf{B}_{3D}$), and ϕ is the phase shift between the 2D and the 3D mode (set to $\frac{1}{2}\pi$ throughout). For the velocity field we have

$$\mathbf{v}(x, y, z, t = 0) = \epsilon_{2D}\,\mathbf{v}_{2D}(z)\,e^{i\alpha x} + \epsilon_{3D}\,\mathbf{v}_{3D}(z)\,e^{i\alpha(x+\phi)+i\beta y}. \tag{1b}$$

The system is governed by the dissipative, incompressible, magnetohydrodynamic (MHD) equations, written in a dimensionless rotation form:

$$\frac{\partial \mathbf{v}}{\partial t} = \mathbf{v}\times\boldsymbol{\omega} - \boldsymbol{\nabla}\boldsymbol{\Pi} + \mathbf{j}\times\mathbf{B} + \frac{1}{S_v}\nabla^2\mathbf{v}, \tag{2a}$$

$$\boldsymbol{\nabla}\cdot\mathbf{v} = 0, \tag{2b}$$

$$\frac{\partial \mathbf{B}}{\partial t} = \boldsymbol{\nabla}\times\mathbf{v}\times\mathbf{B} - \frac{1}{S}\boldsymbol{\nabla}\times\boldsymbol{\nabla}\times\mathbf{B}, \tag{2c}$$

$$\boldsymbol{\nabla}\cdot\mathbf{B} = 0, \tag{2d}$$

where $\mathbf{v}(\mathbf{x}, t) = (u, v, w)$ is the flow velocity, $\boldsymbol{\omega}(\mathbf{x}, t) = \boldsymbol{\nabla}\times\mathbf{v}$ is the vorticity, $\mathbf{B}(x, t)$ is the magnetic field, $\mathbf{j}(\mathbf{x}, t) = \boldsymbol{\nabla}\times\mathbf{B}$ is the electric current density, $\boldsymbol{\Pi}(\mathbf{x}, t)$ is the mechanical pressure + kinetic energy density, S_v is the viscous Lundquist number (with the viscosity assumed to be constant and uniform), and S is the Lundquist number (with the resistivity assumed to be constant and uniform). In this representation, $\mathbf{B}$ is measured in units of the background x magnetic field far from the current sheet. The velocities are measured in units of the Alfvén speed, $C_A = B_0/(4\pi\rho)^{1/2}$, where the mass density ρ is assumed to be constant and uniform. Hence $M_A = 1$. For a characteristic distance L_0 defined by the current sheet width, the time is measured in units of the Alfvén transit time L_0/C_A.

For the primary current sheet basic state we choose

$$U_0(z) = 0, \tag{3a}$$

$$B_{0z}(z) = \tanh z, \tag{3b}$$

$$B_{0y}(z) = C. \tag{3c}$$

https://doi.org/10.1017/S0022377896005247 Published online by Cambridge University Press

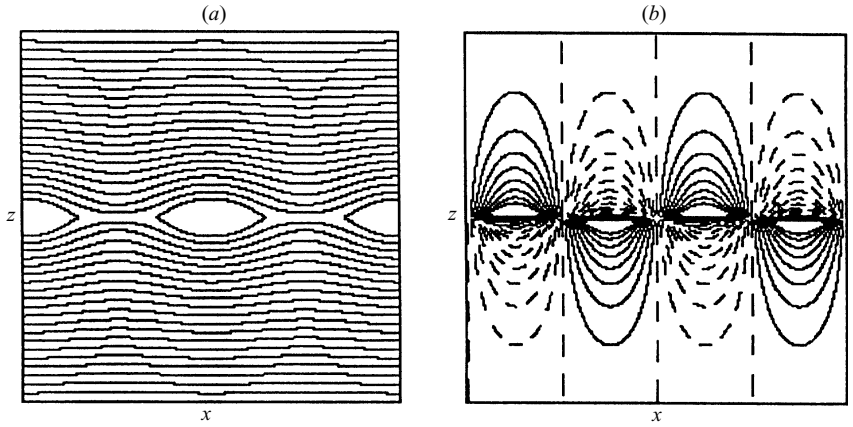


Figure 2. Contour plots showing the basic fields plus a large dose of the primary two-dimensional unstable eigenfunction: (*a*) magnetic vector potential; (*b*) velocity stream function. Two periods in x are shown. Dashed lines indicate a negative value. The fields shown in the contour plots strongly resemble the secondary equilibrium state.

In analogy with the hydrodynamic problems, we refer to the spatial coordinate along the magnetic field (x) as the fieldwise direction, the spatial coordinate across the current sheet (z) as the cross-sheet direction, and the remaining spatial coordinate (y) as the sheetwise direction. We consider a system with periodic boundary conditions in the fieldwise and sheetwise directions. In the cross-sheet direction we want the magnetic field to merge into the background field as it moves away in z from the current sheet. Hence we want to enforce

$$B_x(\pm\infty) = \pm 1, \quad B_y(\pm\infty) = C, \quad B_z(\pm\infty) = 0, \tag{4}$$

where C is a constant. We impose this computationally with free-slip boundary conditions (Orzsag and Pao 1974)

$$\frac{\partial B_x}{\partial z} = \frac{\partial B_y}{\partial z} = B_z = 0 \quad \text{at } L_3, \tag{5a}$$

$$\frac{\partial u}{\partial z} = \frac{\partial v}{\partial z} = w = 0 \quad \text{at } L_3, \tag{5b}$$

where L_3 is the computational boundary in the cross-sheet direction.

The 2D and 3D primary perturbations are determined as solutions of the eigenvalue problem defined by a magnetohydrodynamic generalization of the Orr–Sommerfeld equation, which is derived in the appendix to this paper. These unstable eigenfunctions, along with their growth rates, are shown in Fig. 1. The unstable eigenfunctions resemble the modes studied by Furth *et al.* (1963). For purely 2D disturbances, the electric current sheet primary unstable mode is identical to the neutral sheet primary unstable mode. Only for the 3D case, with finite sheetwise wavenumber β, are there differences. Hence, to facilitate comparison between all of the cases, we use the neutral sheet primary 3D disturbance mode.

Note that the 2D mode growth rate is larger than the 3D mode growth rate.

https://doi.org/10.1017/S0022377896005247 Published online by Cambridge University Press

The decrease in the 3D mode growth rate with increasing β is even larger for the electric current sheet modes. Hence it is justifiable to assume that, all other things being equal, the 2D unstable primary mode should grow up and saturate before the 3D unstable primary mode. In Fig. 2 we show the basic state (2) combined with a large dose of the 2D primary unstable eigenfunction. Two periods in the fieldwise direction x are shown. The state shown in Fig. 2 strongly resembles the 2D saturated state that develops as the 2D primary unstable eigenmodes saturate (Steinolfson and Van Hoven 1983). It has been shown that the shape approximation holds for the neutral sheet (Dahlburg *et al.* 1986). In the remainder of this paper we shall inquire into what happens when the state shown in Fig. 2 is subject to small perturbations in the sheetwise (y) direction. This is the key aspect in which this secondary instability analysis differs from the primary instability analysis, which examines the stability of small perturbations to the basic state given in (2).

3. Numerical results

Next we provide numerical evidence for the existence of a secondary instability of the current sheet and investigate its parametric dependence on B_{0y}. The investigation relies on numerical simulation of (2). We employ a semi-implicit Fourier pseudospectral–Fourier collocation algorithm. The primary disturbances for all of the runs are the 2D and 3D eigenfunctions for the neutral sheet case.

The energy contained in the 3D secondary modes is given by

$$E_{3D} = \frac{1}{2}\int (|\mathbf{B}^{(3)}|^2 + |\mathbf{v}^{(3)}|^2)\, d^3x, \tag{6a}$$

where we obtain $\mathbf{B}^{(3)}$ and the other fields from the following decomposition:

$$\mathbf{B} = B^{(1)}(z,t)\,\hat{\mathbf{e}}_x + \sum_{|m|<M/2} \tilde{\mathbf{B}}^{(2)}_{m0}(z,t)\, e^{i\alpha m x} + \sum_{n=\pm 1}\sum_{|m|<M/2} \tilde{\mathbf{B}}^{(3)}_{mn}(z,t)\, e^{i\alpha m x} e^{i\beta n y}, \tag{7a}$$

$$\mathbf{v} = U^{(1)}(z,t)\,\hat{\mathbf{e}}_x + \sum_{|m|<M/2} \tilde{\mathbf{v}}^{(2)}_{m0}(z,t)\, e^{i\alpha m x} + \sum_{n=\pm 1}\sum_{|m|<M/2} \tilde{\mathbf{v}}^{(3)}_{mn}(z,t)\, e^{i\alpha m x} e^{i\beta n y}, \tag{7b}$$

where the tilde denotes the Fourier coefficient. It can be seen from these formulae that, for example, $\mathbf{B}^{(1)}$ represents the part of the magnetic field that only varies in z, $\mathbf{B}^{(2)}$ represents the part of the magnetic field that varies in x and z, and $\mathbf{B}^{(3)}$ represents the part of the magnetic field that varies in x, y and z. The same is true for $\mathbf{v}$.

Figure 3 shows the total 3D energy (E_{3D}) as a function of time for a series of runs in which B_{0y} is varied. For these runs we have set $S = S_v = 10^3$, $\alpha = \beta = 0.2$, $\epsilon_{2D} = 0.02$ and $\epsilon_{3D} = 10^{-9}$. As previously demonstrated, for $B_{0y} = 0$ there is a secondary instability, which can be shown to be ideal. As seen in Fig. 3, for many values of B_{0y} there is still a secondary instability. However, increasing B_{0y} causes a decrease in the rate of growth of this secondary mode. Furthermore, there is a critical value of B_{0y} above which the secondary instability is stabilized. For the cases shown here, that value is between 1.75 and 2. Note as well that simulations with different values of the Lundquist numbers show that the instability retains its ideal character with non-zero B_{0y}.

https://doi.org/10.1017/S0022377896005247 Published online by Cambridge University Press

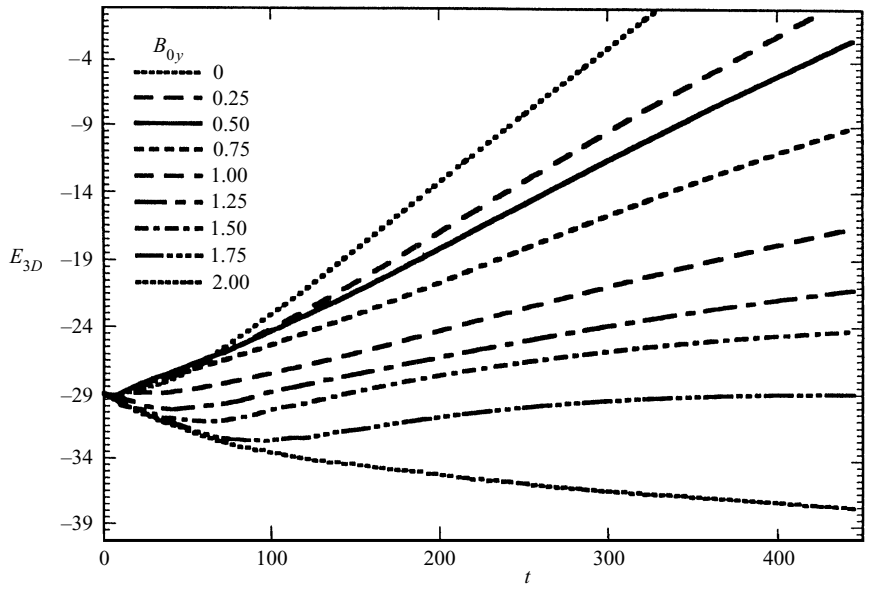


Figure 3. The three-dimensional energy E_{3D} as a function of time t for $B_{0x} = \tanh z$, $S = S_v = 1000$, $\alpha = \beta = 0.2$, $\epsilon_{2D} = 0.02$ and $\epsilon_{3D} = 10^{-9}$. The curves are parametrized by the sheetwise magnetic field strength B_{0y}.

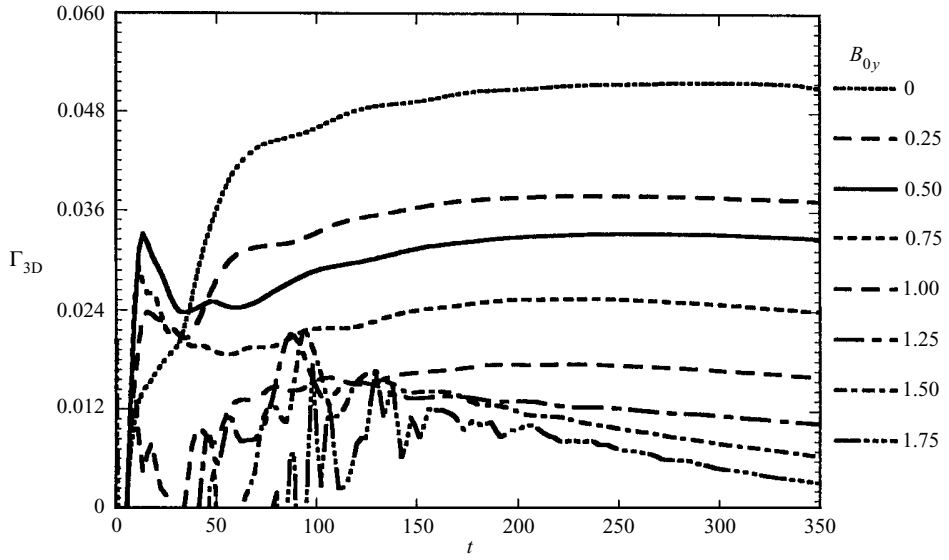


Figure 4. The three-dimensional energy growth rate Γ_{3D} as a function of time t for $B_{0x} = \tanh z$, $S = S_v = 1000$, $\alpha = \beta = 0.2$, $\epsilon_{2D} = 0.02$ and $\epsilon_{3D} = 10^{-9}$. The curves are parametrized by the sheetwise magnetic field strength B_{0y}.

The growth rates for E_{3D} (Γ_{3D}) for these runs are shown in Fig. 4. As expected, the secondary instability growth rate for the neutral sheet ($B_{0y} = 0$) case is the largest, and there is a decrease in (Γ_{3D}) as B_{0y} is increased. Many of these growth rates exceed the 2D primary mode growth rate ($\omega_i = 0.0138$). Since the primary mode growth rate decreases with Lundquist number S, this difference in growth

https://doi.org/10.1017/S0022377896005247 Published online by Cambridge University Press

rates should be magnified at larger S. This decrease is relatively large for small B_{0y}, and becomes smaller as B_{0y} becomes larger: note that Γ_{3D} is cut by more than half for $B_{0y} = 0.75$. We omit the $B_{0y} = 2$ case in this and the following figures because it is very noisy, and obscures the graphical representation of the results from the other cases.

To obtain some information about the stabilization due to increasing B_{0y}, we consider the transfer of energy into and out of the 3D secondary mode. Energy transfer into and out of the 3D modes is governed by the following equation:

$$\frac{dE_{3D}}{dt} = T_{13} + T_{23} + D_3, \tag{9}$$

where T_{13} represents the interaction of the 1D and 3D fields, T_{23} represents the interaction of the 2D and 3D fields, and D_3 represents the Ohmic and viscous diffusion of the 3D field. The energy transfer terms are defined by

$$T_{13} = -\int \mathbf{B}^{[1]} \cdot (\boldsymbol{\nabla} \times \mathbf{v}^{[3]} \times \mathbf{B}^{[3]})\, d^3x. \tag{10a}$$

T_{23} is then given by

$$T_{23} = \int \mathbf{v}^{[3]} \cdot (\mathbf{v} \times \boldsymbol{\omega})\, d^3x + \int \mathbf{v}^{[3]} \cdot [(\boldsymbol{\nabla} \times \mathbf{B}) \times \mathbf{B}]\, d^3x + \int \mathbf{B}^{[3]} \cdot (\mathbf{v} \times \mathbf{B})\, d^3x - T_{13}, \tag{10b}$$

and D_3 is given by

$$D_3 = \frac{1}{R_m} \int |\boldsymbol{\nabla} \times \mathbf{B}^{[3]}|^2\, d^3x + \frac{1}{R} \int |\boldsymbol{\nabla} \times \mathbf{v}^{[3]}|^2\, d^3x, \tag{10c}$$

and

$$\mathbf{B}^{[1]}(z) = [B^{(1)}(z) + B_{00}^{(2)}(z)]\, \hat{\mathbf{e}}_x + [B^{(1)} + B_{00}^{(2)}(z)]\, \hat{\mathbf{e}}_y, \tag{11a}$$

$$\mathbf{B}^{[3]}(x, y, z) = \mathbf{B}^{(3)}(x, y, z), \tag{11b}$$

$$\mathbf{v}^{[3]}(x, y, z) = \mathbf{v}^{(3)}(x, y, z). \tag{11c}$$

To get a normalized growth rate, we compute

$$\gamma = \frac{T_{13}}{2E_{3D}} + \frac{T_{23}}{2E_{3D}} + \frac{D_3}{2E_{3D}} = \tau_{13} + \tau_{23} + \delta_3. \tag{12}$$

It is useful to compute the energy transfer components in this form because then γ can be computed and compared to Γ_{3D} as an accuracy check.

Figure 5 shows τ_{13} as a function of time for the runs shown in Fig. 3. In addition, Fig. 6 shows τ_{23}, and Fig. 7 shows δ_3. First consider the neutral sheet case, with $B_{0y} = 0$. A comparison of Figs 5 and 6 shows that the major contribution to the growth rate γ comes from τ_{13} rather than τ_{23}. By contrast, for $B_{0y} = 0$ the 2D-to-3D energy transfer term τ_{23} remains negative for most of the simulation, and hence the 2D structures in the system, i.e. the magnetic islands, do not provide much energy for the growth of the secondary instability. This indicates that the energy that drives the perturbation is coming from the basic magnetic field given by (11*a*). The dissipative term δ_3 of course remains negative throughout the simulation, since it represents Joule heating and viscous energy losses from the 3D perturbed magnetic and velocity fields.

https://doi.org/10.1017/S0022377896005247 Published online by Cambridge University Press

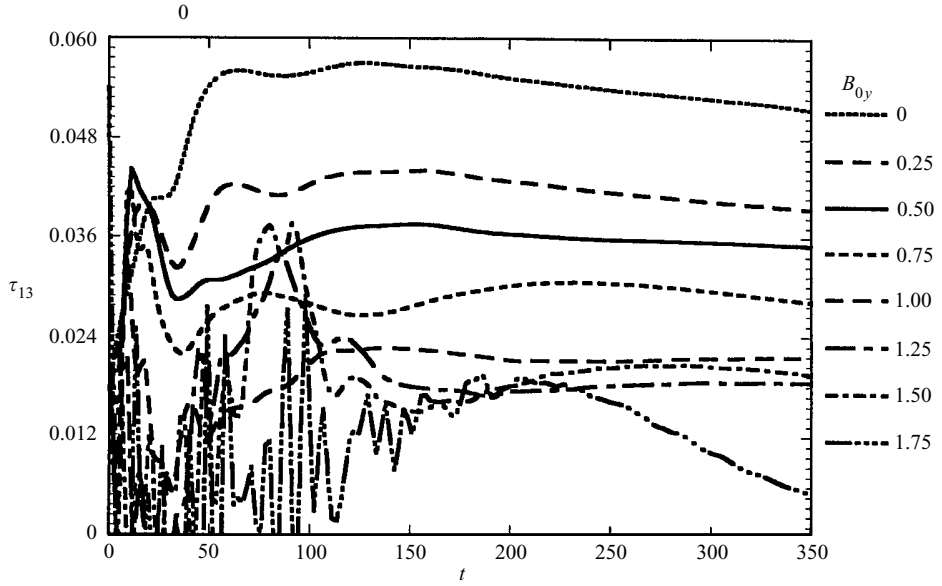


Figure 5. The one- to three-dimensional energy transfer τ_{13} as a function of time t for $B_{0x} = \tanh z$, $S = S_v = 1000$, $\alpha = \beta = 0.2$, $\epsilon_{2D} = 0.02$ and $\epsilon_{3D} = 10^{-9}$. The curves are parametrized by the sheetwise magnetic field strength B_{0y}.

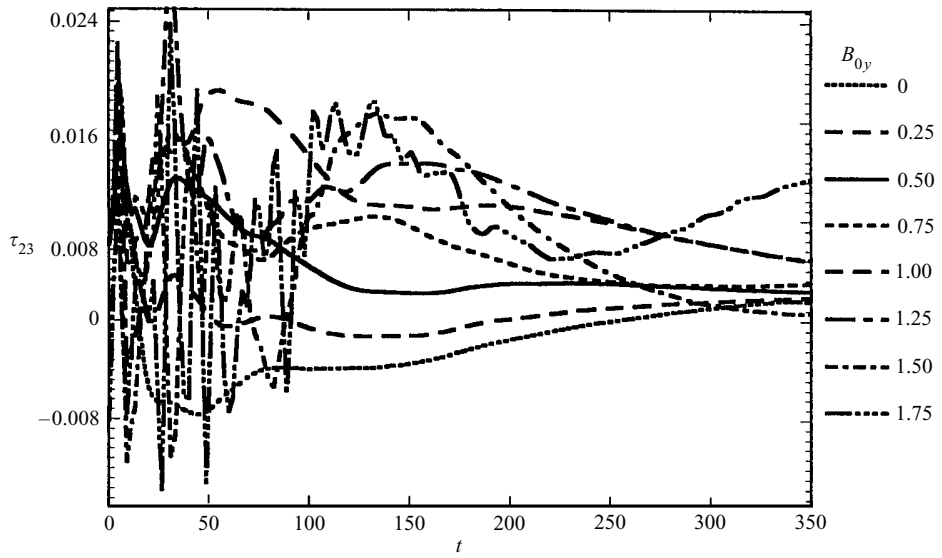


Figure 6. The two- to three-dimensional energy transfer τ_{23} as a function of time t for $B_{0x} = \tanh z$, $S = S_v = 1000$, $\alpha = \beta = 0.2$, $\epsilon_{2D} = 0.02$ and $\epsilon_{3D} = 10^{-9}$. The curves are parametrized by the sheetwise magnetic field strength B_{0y}.

Now consider what happens to τ_{13} as B_{0y} is increased. A comparison of Fig. 5 with Fig. 4 makes it clear that the most significant factor in the decrease of the growth rates shown in Fig. 4 is a decrease in τ_{13} as B_{0y} is increased. As B_{0y} is increased, there is a monotonic decrease in τ_{13} until $B_{0y} = 1.25$; then τ_{13} jumps around somewhat.

https://doi.org/10.1017/S0022377896005247 Published online by Cambridge University Press

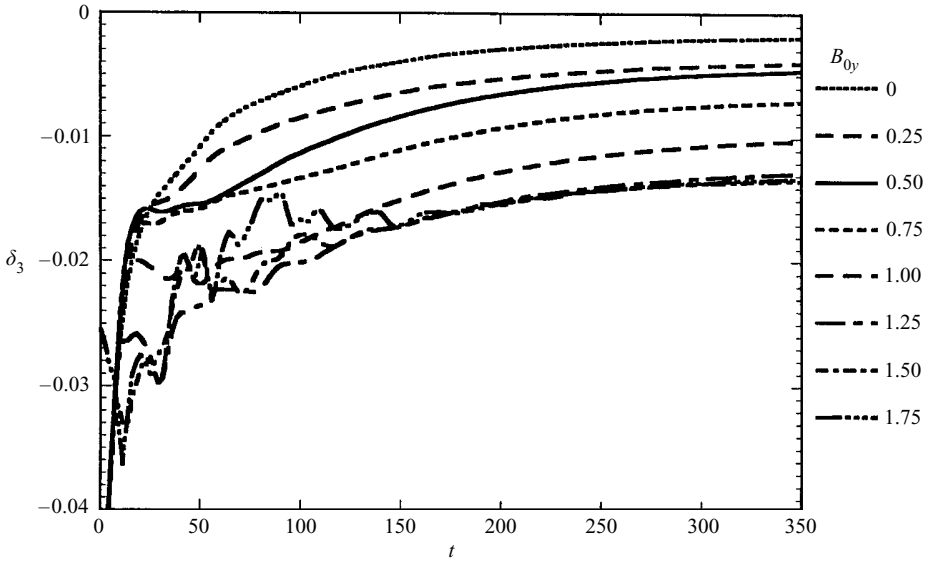


Figure 7. The three-dimensional diffusion δ_3 as a function of time t for $B_{0x} = \tanh z$, $S = S_v = 1000$, $\alpha = \beta = 0.2$, $\epsilon_{2D} = 0.02$ and $\epsilon_{3D} = 10^{-9}$. The curves are parametrized by the sheetwise magnetic field strength B_{0y}.

Figure 6 shows τ_{23}, which remains relatively unchanged as B_{0y} is changed (the values on the ordinates of Figs 5 and 6 should be compared). It is seen that for cases with small B_{0y}, τ_{23} is small compared with τ_{13}. For large B_{0y}, τ_{23} becomes positive and contributes a fraction toward the positive Γ_{3D}.

Finally, Fig. 7 shows the 3D energy diffusion term δ_3 as a function of t, parametrized by B_{0y}. Again, the ordinate of Fig. 7 should be compared with that of Fig. 5. In Fig. 7 we see that the magnitude of δ_3 increases as B_{0y} is increased until $B_{0y} \approx 1.25$. The dissipation δ_3 holds at approximately the same value until $B_{0y} = 2$, at which value it decreases in magnitude for the stabilized secondary mode. Hence δ_3 also contributes to the stabilization of Γ_{3D}.

4. Conclusions

In this paper we have examined the transition to turbulence via secondary instabilities of magnetic reconnection in the electric current sheet. We have shown that a secondary instability exists for the electric current sheet, extending the conjecture of Montgomery (1984) to the electric current sheet. The growth rate for this new secondary mode decreases as the sheetwise component of the basic magnetic field is increased. Furthermore, if the sheetwise magnetic field is increased to a large enough value, the secondary mode is stabilized. The most significant factor in the diminishing of the secondary mode growth rate is a decrease in the energy transferred from the 1D field to the 3D perturbed fields. A lesser factor is an increase in the magnitude of the 3D perturbed Ohmic and viscous energy dissipation.

The analysis in this paper has been limited to cases where the secondary mode perturbation remains small. It remains to be seen what happens when these perturbations attain finite amplitudes. Another issue to consider is the

https://doi.org/10.1017/S0022377896005247 Published online by Cambridge University Press

evolution of more complex perturbations than are considered here, i.e. to consider the evolution of the electric current sheet as an initial value problem involving either infinitesimal perturbations (Dahlburg 1994) or finite-amplitude perturbations.

Acknowledgements

We thank S. K. Antiochos for suggesting this problem. The numerical calculations reported here were performed on the NASA Ames Research Center Cray C90 supercomputer. This work was supported by the NASA Space Physics Theory Program and the Office of Naval Research.

Appendix. Linearized equations for primary instability

After linearizing (2*a–d*) about the basic state given in (3), we assume that the first-order terms can be decomposed in the following manner:

$$f'(x,y,z,t) = \tilde{f}(z)\, e^{i\alpha x + i\beta y - i\omega t}, \tag{A 1}$$

in which α is the fieldwise wavenumber, β is the sheetwise wavenumber and ω is the complex growth rate. After eliminating the pressure, the primary linear perturbations that we shall employ are unstable eigenfunctions of the following equations, where $D \equiv d/dz$ and the tildes have been dropped:

$$(D^2-k^2)^2 w = -i\omega R(D^2-k^2) w + iRM_A^2[(D^2F) b_z - F(D^2-k^2) b_z], \tag{A 2a}$$

$$(D^2-k^2+i\omega R_m) b_z = -iR_m F w, \tag{A 2b}$$

with the boundary conditions

$$w\pm(\infty) = Dw(\pm\infty) = b_z(\pm\infty) = 0. \tag{A 3c}$$

In these equations $k^2 = \alpha^2+\beta^2$ and $F = \alpha B_{0x} + \beta B_{0y}$.

The linear equations are solved using the Chebyshev–τ technique, with the mesh stretched in the vertical direction by a hyperbolic mapping.

In three spatial dimensions, to obtain the other components of the fields, we must solve a perturbed vorticity (or Squire) equation,

$$(D^2-k^2)\zeta + iM_A^2 RF\xi = -i\omega R\zeta + RM_A^2 (DP) b_z, \tag{A 3a}$$

and a similar equation for the perturbed electric current,

$$(D^2-k^2)\xi + iR_m F\zeta = -i\omega R_m \xi + R_m (DP) w, \tag{A 3b}$$

with the boundary conditions

$$\zeta(\pm\infty) = \xi(\pm\infty) = 0. \tag{A 3c}$$

In these equations $P = \beta B_{0x} - \alpha B_{0y}$, $\xi = \beta b_x - \alpha b_y$ and $\zeta = \beta u - \alpha v$. The remaining field components can then be determined using the solenoidality relations for the velocity and magnetic field.

References

Carbone, V., Einaudi, G. and Veltri, P. 1987 *Solar Phys.* **111**, 31.

Dahlburg, R. B. 1994 *Phys. Plasmas* **1**, 3053.

Dahlburg, R. B. and Karpen, J. T. 1994*a* *Space Sci. Rev.* **70**, 93.

https://doi.org/10.1017/S0022377896005247 Published online by Cambridge University Press

Dahlburg, R. B. and Karpen, J. T. 1994*b* *Astrophys. J.* **434**, 766.

Dahlburg, R. B., Zang, T. A., Montgomery, D. and Hussaini, M. Y. 1983 *Proc. Natl Acad. Sci. USA* **80**, 5798.

Dahlburg, R. B., Zang, T. A. and Montgomery, D. C. 1986 *J. Fluid Mech.* **169**, 71.

Dahlburg, R. B., Antiochos, S. K. and Zang, T. A. 1992 *Phys. Fluids* **B4**, 3902.

Dahlburg, R. B., Antiochos, S. K. and Zang, T. A. 1993 *Physics of Solar and Stellar Coronae: G. S. Vaiana Memorial Symposium* (ed. J. L. Linsky and S. Serio), p. 611. Kluwer, Dordrecht.

Furth, H. P., Killeen, J. and Rosenbluth, M. N. 1963 *Phys. Fluids* **6**, 459.

Metcalfe, R. W., Orszag, S. A., Brachet, M. E., Menon, S. and Riley, J. J. 1987 *J. Fluid Mech.* **184**, 207.

Montgomery, D. 1984 *Spectral Methods for Partial Differential Equations* (ed. R. G. Voigt, D. Gottlieb and M. Y. Hussaini), p. 165. SIAM, Philadelphia.

Montgomery, D. 1989 *Lecture Notes on Turbulence* (ed. J. R. Herring and J. C. McWilliams), p. 75. World Scientific, Singapore.

Montgomery, D. C., Dahlburg, J. P. and Dahlburg, R. B. 1987 *Bull. Am. Phys. Soc.* **32**, 1819.

Orszag, S. A. 1971 *J. Fluid Mech.* **50**, 689.

Orszag, S. A. and Pao, Y.-H. 1974 *Turbulent Diffusion in Environmental Pollution* (ed. F. N. Frenkel and R. E. Munn), p. 225. Academic Press, New York.

Orszag, S. A. and Patera, A. T. 1983 *J. Fluid Mech.* **128**, 347.

Steinolfson, R. S. and Van Hoven, G. 1983 *Phys. Fluids* **26**, 117.

Strauss, H. R. 1986 *Phys. Fluids* **29**, 3668.

Strauss, H. R. 1988 *Astrophys. J.* **326**, 412.

https://doi.org/10.1017/S0022377896005247 Published online by Cambridge University Press